Available online at www.sciencedirect.com

ScienceDirect

journal homepage: www.elsevier.com/locate/issn/15375110

Special Issue: Sensing and Control of Crop Water Status

Research Paper

Linking thermal imaging and soil remote sensing to enhance irrigation management of sugar beet

L. Quebrajo [a], M. Perez-Ruiz [a,*], L. Pérez-Urrestarazu [a], G. Martínez [b], G. Egea [a]

[a] Universidad de Sevilla, Área de Ingeniería Agroforestal, Dpto. de Ingeniería Aeroespacial y Mecánica de Fluidos, Spain

[b] Universidad de Córdoba, Dpto. de Agronomía, Spain

ARTICLE INFO

Article history:
Published online 2 September 2017

Keywords:
Remote sensing
Unmanned aerial vehicle (UAV)
Precision agriculture
Aerial image
Crop water stress index (CWSI)

The use of reliable information and data that are rapidly and easily acquired is essential for farm water management and appropriate irrigation strategies. Over the past decade, new advances have been made in irrigation technology, such as platforms that continuously transmit data between irrigation controllers and field sensors, mobile apps, and equipment for variable rate irrigation. In this study, images captured with a thermal imaging camera mounted on an unmanned aerial vehicle (UAV) were used to evaluate the water status of sugar beet plants in a plot with large spatial variability in terms of soil properties. The results were compared with those of soil moisture measurements. No direct relationship was observed between the water status of the soil and that of the crops. However, the fresh root mass and sugar content tended to decrease when higher levels of water stress were detected in the crop using thermal imaging, with coefficients of determination of 0.28 and 0.94 for fresh root mass and sugar content, respectively. Differences were observed between different soil types, and therefore different irrigation strategies are needed in highly heterogeneous plots.

1. Introduction

Farmers, cooperatives and agricultural consultants are facing radical changes regarding the methods employed to collect, analyse, and use information to add value to their production outputs. Over the past 20 years, we have observed increasing interest in farm- and block-level precision agriculture (Blackmore, Godwin, & Fountas, 2003; Zude-Sasse, Fountas, Gemtos, & Abu-Khalaf, 2016); however, the next 20 years will give rise to canopy-, branch-, and even fruit-level production practices that will demand a new farming mentality (Krishna, 2016, chap. 5). Field sensors will provide terabytes of quantitative and qualitative information about crops, such as nutrients levels and plant and soil moisture status, and about orchards, such as the three-dimensional canopy shape, the mass and size of each fruit, as well as the number of fruits per plant. Amassing this information into a coherent database that can be rapidly and easily used to make informed

* *Corresponding author*. Ctra. Utrera, km 1, Sevilla, 41013, Spain. Fax: +34 954 481389.
E-mail address: manuelperez@us.es (M. Perez-Ruiz).
http://dx.doi.org/10.1016/j.biosystemseng.2017.08.013

decisions on what, when, where, and how to plant, irrigate, prune, thin, treat and harvest each crop will soon be one of the fundamental challenges for farmers to address (Cox, 1996). This scenario allows farmers to move from intuitive decision making to analytical decision making.

Irrigation accounts for 70% of the freshwater (watercourses and groundwater) used worldwide, which is three times more than 50 years ago. During recent droughts, such as those in California (from 2013 to 2015) or Spain, continuous water deficits have increased from 15 to 60 months (Lopéz-Moreno et al., 2009); these droughts highlight the need for precision irrigation techniques to improve water use efficiency so that the resource is applied exactly at the right location, time and rate. The possibilities introduced by the use of remote sensing include precise water management within a plot. Therefore, different irrigation strategies can be followed based on the spatial variability of the soil and crop conditions. Because of this variability, the actual water requirements of crops may change within the same plot. In this case, the challenge for precision irrigation is the development of methodologies to acquire the required information that will allow uniform management within demarcated areas in the plots and the validation of protocols that enable precise irrigation in various sub-units.

Soil moisture monitoring through instruments placed in a few locations in a field has been argued to have important disadvantages that are primarily related to representativeness and the fact that crop water status depends on other factors in addition to soil moisture content (Jones, 2004). The water status of plant tissues, which is commonly measured in terms of water potential (Jones, 1992), can be used as a precise indicator for irrigation scheduling (Jones, 2004). Pressure chambers (Scholander, Hammel, Bradstreet, & Hemmingsen, 1965) have been widely employed to measure leaf water potential for water deficit determination and irrigation scheduling. Although this method is a reliable measure of plant water status, it is highly time consuming and labour intensive, which results in inadequate sampling (Cohen, Alchanatis, Meron, Saranga, & Tsipris, 2005). Moreover, this method is not feasible for measuring the water potential of certain leaf types, such as those of sugar beet.

Measurement of canopy temperature has been proposed as an alternative method of determining water potential (Bellvert et al., 2016). As water stress is induced, the stomata close, transpiration rates decrease and evapotranspirative cooling is reduced, causing leaf temperatures to increase (Maes & Steppe, 2012). Idso, Jackson, Pinter, Reginato, and Hatfield (1981) and Jackson, Idso, Reginato, and Pinter (1981) suggested the use of the crop water stress index (CWSI) as an indicator of plant water stress. Sensing the canopy temperature using infrared sensors or imaging has shown good potential for calculating the CWSI and estimating the plant water status for irrigation scheduling in cotton, corn, sunflower, grapevine, and pistachios (Gonzalez-Dugo, Moran, Mateos, & Bryant, 2006; Payero, Tarkalson, & Irmak, 2006; Möller et al., 2007; Testi, Goldhamer, Iniesta, & Salinas, 2008; Taghvaeian, Comas, DeJonge, & Trout, 2014). Although a non-water-stressed baseline, i.e., a wet reference, to calculate the CWSI was reported for sugar beet (Idso, 1982), the upper baseline, i.e., a water-stressed baseline or dry reference, contains some uncertainty, with most studies assuming a rather arbitrary fixed temperature increment above air temperature to represent the temperature of non-transpiring leaves; values approximately 5 °C above air temperature are often used. Alternatively, the degrees above non-stressed (DANS) index, which is a simplified version of the CWSI that is based only on the difference between the stressed and non-stressed canopy temperatures, can be used (Taghvaeian et al., 2014; DeJonge, Taghvaeian, Trout, & Comas, 2015). However, to the best of our knowledge, thermal sensing has not been applied to optimise sugar beet irrigation. Sugar beet is considered a highly water-consuming crop (Fabeiro, Martin de Santa Olalla, Lopez, & Dominguez, 2003), and its future in drought-prone areas with limited water resources could be compromised if crop productivity is not maintained under expected reductions in available irrigation water. To attain this objective, farmers are obliged to implement precision irrigation tools, such as thermal-based crop stress sensing, which may overcome the drawbacks of soil moisture and leaf water status monitoring, especially when remotely monitoring large areas of crops.

The earth-emitted thermal energy is a function of the surface temperature (Ts) and the surface emissivity, where emissivity is a material property that ranges in value from 0 to 1 (Snyder & Zhengming, 1998). Since remote sensors can detect and quantify the heat emitted from the earth, the surface temperature can be easily determined. Thermal images captured using micro-unmanned aerial vehicles (UAVs) have considerable advantages over manual infrared thermometers, which require considerable effort and provide limited representation of the whole field, and thermal imaging satellite data in which the spatial and temporal resolution is not sufficient for most irrigation applications. For small- and medium-sized plots, UAVs have a competitive advantage over large, autonomous aerial platforms, such as manned aircraft carrying considerable amounts of remote sensing equipment.

The goal of this study was to evaluate the use of thermal images captured using a micro-UAV to predict variations in crop water use due to soil variability and irrigation management. This method can subsequently be used as a decision support tool for the efficient irrigation management of sugar beet.

2. Materials and methods

2.1. Field description and experimental conditions

Field tests were conducted in a commercial sugar beet field (*Beta vulgaris* L., ssp. *vulgaris* var. *altissima*) during the 2014/2015 growing cycle (i.e., from October to July). The field was located in Cadiz, SW Spain (Latitude, 36.6965397° N; Longitude, 6.3184375° W). The experimental field covered an area of approximately 12 ha and was irrigated with a sprinkler system consisting of a triangular arrangement of emitters spaced 12 m apart along the laterals; the laterals were also spaced 12 m apart. The sprinkler wetting radius was approximately 12 m at a working pressure head of 30 m. In southern Spain, sugar beet is sown in autumn. In the experimental field, the crop was planted in mid-November at a depth of 25 mm with

120 mm between plants and 500 mm between plant rows. The climate of the study area is Mediterranean, with rainfall occurring normally from late September to May. The average annual reference evapotranspiration (ET_0) and precipitation values calculated for the 2012–2015 period from data recorded at a nearby weather station belonging to the Agroclimatic Information Network of the Andalusia government (36° 43′ 08″ N, 06° 19′ 48″ W) were 1273 mm and 471 mm, respectively. Table 1 shows the weather data recorded over the experimental growth season (2014–2015).

2.2. Soil characteristics and variability

Soil variability was characterised by conducting two complementary tests. Soil texture was measured based on thirty soil samples collected to a depth of 300 mm using a soil auger. Soil analyses were performed in the Centre for Research, Technology and Innovation (CITIUS Laboratory) at the University of Seville. Systematic sampling was performed by maintaining a fixed distance between two sampling points (using a net or mesh). All samples were georeferenced using a differential-global navigation satellite system (DGNSS) receiver and geographic information system (FarmWorks, Trimble Navigation Ltd., Sunnyvale, CA, USA), and distribution maps of different soil properties were compiled using a kriging technique (Goovaerts, 1997).

Apparent electrical conductivity (ECa) was measured using an EMI Dualem-21S sensor (DUALEM, Milton, Canada) operated at a height of 75 mm above the soil surface and sheltered in a customised polyvinyl chloride case. The equipment was pulled by an all-terrain vehicle (Fig. 1a) and was coupled to a real-time kinematic differential global positioning system (Trimble, Sunnyvale, CA) to collect samples over a 12-ha swath of the field site. Measurements were collected in parallel swaths from NE to SW separated by 10 m with the aid of a guidance system; points within a swath were separated by 1–2 m. We also collected samples along 23 NW to SE swaths to increase the sample density. The sensor was operated at a fixed frequency of 9 kHz and consisted of a transmitter coil at one end and four receiver coils that were separated from the transmitter coil by 1, 1.1, 2, and 2.1 m. The receiver coils were oriented in a perpendicular (PrP) or horizontal co-planar (HCP) configuration with respect to the transmitter coils. Each transmitter–receiver combination provided integrated ECa values for the corresponding explored soil volumes; these values depended on the exploration depth of each signal. The effective depth of exploration is the depth over which an array accumulates 70% of its total sensitivity, which also depends strongly on the ECa of the soil (Callegary, Ferre, & Groom, 2007). The theoretical exploration depths for the 1.1- and 2.1-m HCP and the 1- and 2-m PrP coil combinations were 0.5, 1.0 and 1.6 and 3.2 m, respectively. At high values of true conductivity, the sensor has a non-linear response, and ECa is increasingly underestimated for a given frequency and intercoil spacing (McNeill, 1980). Beamish (2011) proposed a correction procedure involving a least-squares polynomial fitted to the theoretical deviation of the linear relationship between LIN-approximated ECa and the true conductivity of the coil configurations to allow for the correction of the LIN approximation breakdown. This approach was adopted in the present study, and the corrected LIN-approximated ECa is used hereafter. The coefficients used for the polynomial fitting are available in Delefortrie et al. (2014). The final transformation applied to the raw ECa data accounted for the soil temperature effects. A reference temperature of 25 °C is typically used (Corwin & Lesch, 2005):

$$ECa_{25} = ECa\left[0.447 + 1.4034e^{-\left(\frac{T}{26.815}\right)}\right] \quad (1)$$

where ECa_{25} is the standardised ECa at a temperature of 25 °C, and T is the soil temperature in °C. To simplify the nomenclature, we use ECa as the temperature-corrected ECa (ECa_{25}) reading. The average soil temperature at a depth of 0–0.30 m, obtained from 30 samples collected across the field, was used. Given the high correlations between signals observed in the field (correlation coefficients ranging from 0.9 to 0.94), we used the 1.1 HCP signal that best represented the rooting depth of the sugar beet crop. The FAO has established a range of maximum effective rooting depths for sugar beet, i.e., 0.7–1.2 m (Allen, Pereira, Raes, & Smith, 1998). The ECa data were filtered to remove spurious errors and were interpolated by means of ordinary block kriging on a 2 × 2-m grid to create maps for the four ECa signals using the geostatistical analyst in ArcGIS (ESRI, Redlands, CA) (Fig. 1b). We used an anisotropic spherical model to fit the variogram with a lag size of 1.5 m, range of 75 m, sill of 1663 (mS m^{-1})^2 and 115° as its main direction. A cross validation of the interpolation yielded a root mean squared error of 6.5 mS m^{-1}.

Table 1 – Monthly meteorological variables measured during the 2014/2015 sugar beet growing season at a nearby standard weather station of the Agroclimatic Information Network of the Andalusia government. P (mm): rainfall; T_m (°C): mean air temperature; RH_m (%), mean relative humidity; u (m s^{-1}), mean wind speed; R_s (MJ m^{-2} day^{-1}), solar radiation; ET_0 (mm day^{-1}), mean FAO-Penman Monteith reference crop evapotranspiration.

Date	P	T_m	RH_m	u	R_s	ET_0
	mm	°C	%	m s^{-1}	MJ m^{-2} day^{-1}	Mm day^{-1}
Oct-14	66	20.5	71.3	2.1	15.0	3.4
Nov-14	185	15.4	82.2	2.7	9.8	1.9
Dec-14	49	9.9	87.9	2.3	8.7	1.2
Jan-15	151	9.7	85.4	2.9	10.3	1.5
Feb-15	17	10.9	77.9	3.3	13.2	2.2
Mar-15	50	13.1	79.1	2.3	17.4	3.0
Apr-15	35	16.3	76.3	3.2	21.5	4.1
May-15	7	20.7	59.8	2.6	27.2	6.2
Jun-15	9	22.4	60.4	2.5	26.8	6.2
Jul-15	9	24.7	69.0	1.8	28.7	6.3

2.3. Mapping soil heterogeneity and selection of experimental plots

The soil texture maps generated using Farm Works (Trimble Navigation Ltd.) mapping software (Fig. 1c) showed strong soil variability. Two zones of extremely high soil texture variability were identified; one with prevailing clayey soil, and the other with sandy soil (Fig. 1c). Within each of the selected

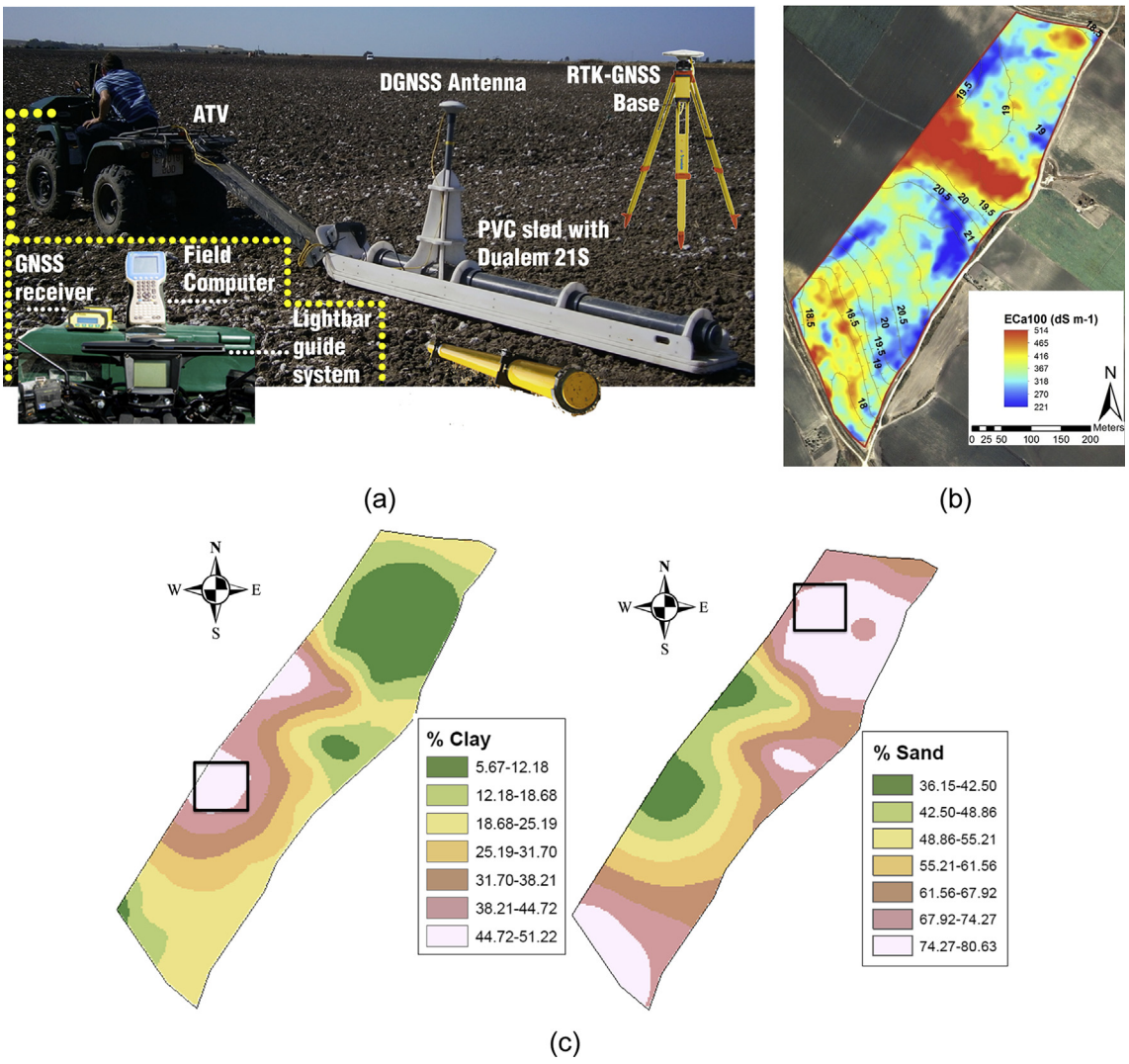

Fig. 1 – a) Dualem sensor. b) CEa map obtained at a depth of 1000 mm. c) Clay and sand content maps. The squares indicate the selected zones.

areas (clayey and sandy zones), two experimental plots (4 in total) covering an area of approximately 72 m^2 (i.e., the area within three adjacent sprinklers, with a triangular arrangement of sprinklers) were established. The visual confirmation of the ECa maps (Fig. 1b) with the soil texture maps confirmed that the selected clayey and sandy zones presented relatively uniform medium and low range ECa values, respectively.

2.4. *Soil moisture measurement*

Soil moisture was measured in the 0–1000-mm soil profile during the study period using a multi-sensor PR-2 profile probe (Delta-T Devices, Ltd., Cambridge, UK). Two epoxy-fibreglass access tubes with a rubber-sealing plug were buried in each experimental plot. The PR-2 is a polycarbonate rod with six pairs of stainless steel rings at 100, 200, 300, 400, 600 and 1000 mm, and soil moisture was measured at these depths. The PR-2 probe was calibrated for each soil zone (i.e., the selected clayey and sandy zones), and the manufacturer's equation (Qi & Helmers, 2010) was applied to convert the permittivity into volumetric soil water content. For the calibration, undisturbed soil samples were collected near the access tubes at the end of the growing cycle over several days to ensure a broad range of soil moisture conditions. Bulk density and volumetric moisture content were determined for each sample. The moisture measurements collected using the PR-2 probe and those obtained in the laboratory were used to determine the calibration curves for each soil type. Once calibrated, the soil moisture measurements in the 0–1000-mm soil profile were used to calculate changes in the relative extractable water (REW) for all experimental plots using the following expression:

$$REW = \frac{R - R_{min}}{R_{max} - R_{min}} \quad (2)$$

where R is the soil moisture content, and R_{max} and R_{min} are the soil moisture contents at the field capacity and wilting point, respectively. The values for R_{max} and R_{min} were determined using the Rosetta model, which is based on the van Genuchten model (Van Genuchten, 1980), and the soil physical properties

measured in each selected zone (i.e., sand, clay and silt fraction; bulk density).

2.5. Thermal imaging and Unmanned aerial vehicle description

Thermal images of the sugar beet fields were acquired using an uncooled Tau 2324 thermal camera (FLIR Systems, Inc., Oregon, USA). The main characteristics of the camera are summarised in Table 2. The accuracy of thermal measurements performed using this type of camera mounted on a UAV has been reported to be approximately 1K (Berni, Zarco-tejada, Suárez, & Fereres, 2009).

The camera was installed in a vertical orientation in the middle of the bottom of the UAV, which was a small Phantom 2 multi-rotor copter (SZ DJI Technology Co., Ltd., Shenzhen, China) equipped with a GNSS receiver. The UAV, which had a flight duration of 25 min and a remote control range of 1000 m in open spaces, was controlled by the DJI iPad Ground Station application.

The UAV was flown across the experimental field on six clear-sky days over the period from day of year (DOY) 86 to DOY 167. The flights, which were performed at solar noon, measured surface temperature over the four experimental plots at several heights (5 m, 10 m, 20 m, 30 m and 40 m) above the ground level. The flight time over the different experimental plots and at several heights did not exceed 30–40 min in order to minimise the differences in weather conditions during the period of measurement. The thermal images were acquired at a rate of 9 frames per second and were stored on-board in a raw format with 14-bit radiometric resolution. A total number of 50 selected thermal images were analysed during the growth season.

The thermal images captured by the UAV were used to calculate the mean sugar beet temperature of each experimental plot by averaging the temperature of the pure vegetation pixels. Pure vegetation pixels were extracted from the thermal image using a segmentation algorithm written in R (R Core Team, 2015) and based on a histogram analysis of pixels from each thermal image (Fig. 2) and the 'full width at half maximum' (FWHM) rule. The FWHM rule allows identification of pixels with high probability of being pure vegetation, as described elsewhere (Rud et al., 2015; Käthner et al., 2017). The assessment of crop water status was based on the difference between the average temperature of the vegetation cover and the prevailing air temperature at the time of flight (ΔT), measured using the air temperature sensor (model HMP45C, Vaisala, Helsinki, Finland) installed at the nearby weather station (absolute precision of ±0.2 °C). Values of ΔT were also used to determine a cumulative integral of the degree of crop water stress throughout the irrigation season. The difference between ΔT and the corresponding value for a non-stressed canopy provides the difference in canopy temperature, or degree of stress, for a specific sampling date. This indicator, DANS, was adapted by DeJonge et al. (2015) to integrate the impact of water stress throughout a whole day. In this study, an expression analogous to the water stress integral (WSI), originally proposed by Myers (1988) for predawn leaf water potential measurements, was used to determine the cumulative integral of water stress over the entire irrigation season as measured by differences in canopy temperature:

$$WSI(^{\circ}C\ day) = \sum_{i=0}^{i=t} (\Delta T_{i,i+1} - c_{i,i+1})n \quad (3)$$

where t represents the number of ΔT measurements (t = 6), in agreement with the number of flights conducted; $\Delta T_{i,i+1}$ is the average ΔT for any interval i, i + 1; $c_{i,i+1}$ is the average of the non-water-stressed ΔT values for any period i, i + 1; and n is the number of days in the interval. The c values were obtained from the non-water-stressed baseline (NWSB) derived by Idso (1982) to calculate the CWSI for sugar beet:

$$c_i = a + bVPD_i \quad (4)$$

where VPD_i represents the prevailing vapour pressure deficit (kPa) at the time of flight on the ith measurement day, and *a* and *b* are two parameters obtained empirically for each species under specific environmental conditions. The *a* and *b* values for sugar beet on sunny days are a 2.50 and −1.92, respectively (Idso, 1982). The VPD and air temperature data at a height of 2 m were obtained from a nearby weather station belonging to the Agroclimatic Information Network of the Andalusia government.

The NWSB from Idso (1982) was also used to calculate the CWSI of the ith sampling day as follows:

$$CWSI = \frac{\Delta T_i - c_i}{\Delta T_{dry,i} - c_i} \quad (5)$$

where $\Delta T_{dry,i}$ represents the maximum ΔT, which corresponds to a non-transpiring canopy. In this case study, it was found that the sugar beet leaf temperature could reach up to 8 °C above air temperature; consequently, a constant $\Delta T_{dry,i} = 8$ °C was used. Similar $\Delta T_{dry,i}$ values have been found for other herbaceous crop species (Rud et al., 2014).

2.6. Irrigation strategy

Two experimental plots were established in each of the selected soil zones, i.e., the clayey and sandy areas of the experiment. In each soil zone, one of the plots was irrigated following the criteria used by local farmers (WW, to indicate presumed well-watered conditions), and in the other experimental plot, two water stress cycles were imposed by withholding irrigation through nozzle blinding of adjacent sprinklers for approximately three weeks per cycle (WS, to indicate water-stressed conditions). A recovery period of 24 days was established between both water deficit cycles. The irrigation depths applied to the WW and WS plots over the

Table 2 – Thermal camera technical data.

	Camera features
Scene range	−25 °C to 135 °C
Detector	Vanadium Oxide (VOx) microbolometer
FPA/video display format	324 × 256 pixels
Infrared lens	9 mm f/1.25
Temperature sensitivity	<50 mK
Wide field of view	48° × 37°
Full frame rates:	30/60 Hz
Pixel pitch	25 μm

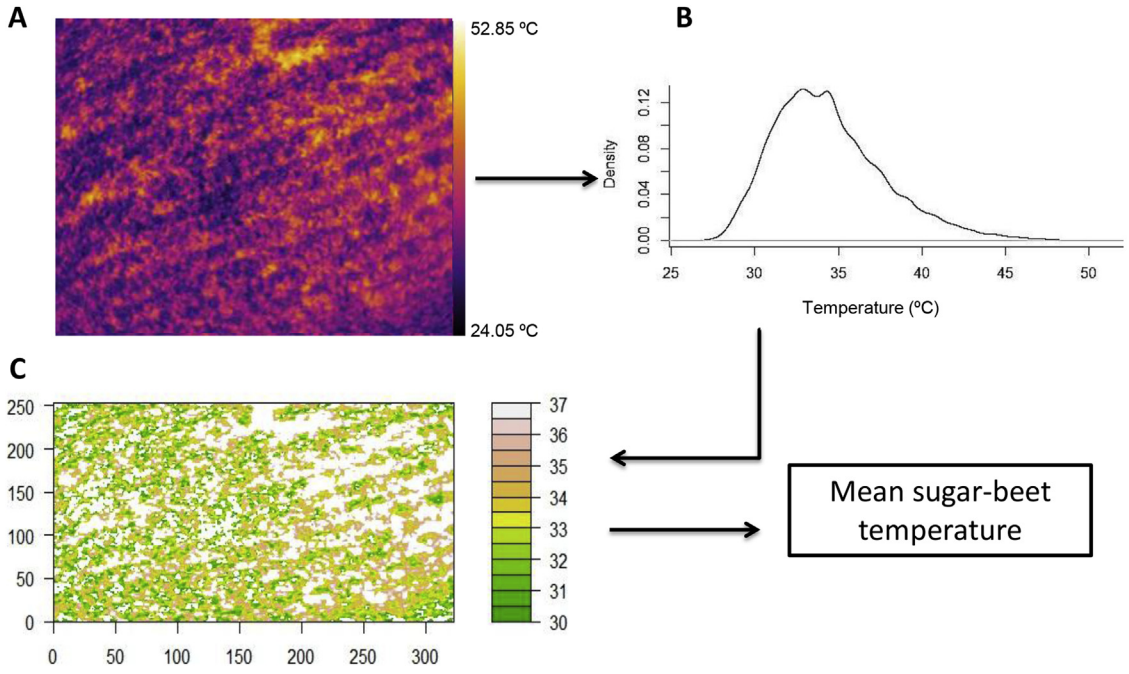

Fig. 2 – Thermal image processing performed in this field trial to derive the mean sugar beet temperature in each experimental plot. The segmentation algorithm is based on a histogram analysis and the FWHM rule. (A) Thermal image of a sugar beet field plot; (B) distribution of temperature in the thermal image depicted as a density histogram; (C) segmented thermal image in which the regions of interest have been selected.

entire growing season were 320 mm and 170 mm, respectively. The irrigation depth applied during each irrigation event was 30 mm, except for one where 20 mm was applied. Irrigation frequencies were determined from the cumulative crop water requirements calculated following the FAO-Penman-Monteith method (Allen et al., 1998).

2.7. *Production*

Sugar beet yield was evaluated in the four experimental plots by manual harvesting six samples per experimental plot at the end of the growing season (early July). Fresh root mass (t ha^{-1}), sugar recovery (%) and sugar content (t ha^{-1}) were determined for each sample.

2.8. *Statistical analyses*

Analysis of variance (ANOVA) performed with the statistical package Statgraphics (Statgraphics Centurion XV) was used to compare the components and yield and between treatments. The relationships between yield, components and the water stress integral were evaluated using linear regression analysis in Statgraphics software.

3. Results

3.1. *Soil moisture*

The soil moisture dynamics of the four selected plots are shown in Fig. 3. The WW_{Sand} plot maintained REW values close to one (field capacity) throughout the study period. However, the WW_{Clay} plot could not maintain field capacity conditions throughout the irrigation season, and REW decreased to approximately 0.6 during the period from DOY 80 to 125, even though the irrigation scheduling in both the WW_{Clay} and WW_{Sand} plots was similar.

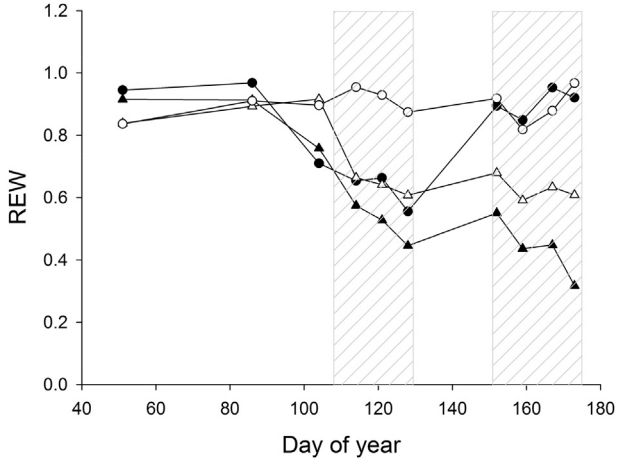

Fig. 3 – Seasonal time courses of the relative extractable water fraction (REW) in the 0–1000-mm soil profile of the four study plots. Each point represents the average of two measurements per plot. The hatched areas indicate the periods during which irrigation was withheld in the WS_{Clay} and WS_{Sand} plots. Definition of symbols: filled triangles (WS_{Clay}), hollow triangles (WS_{Sand}), filled circles (WW_{Clay}), hollow circles (WW_{Sand}).

The REW dynamics in the WS_{Sand} and WS_{Clay} plots were similar throughout the study period, although WS_{Clay} exhibited REW values that were consistently 15–20% lower than those observed in WS_{Sand} (Fig. 3). The restarting of irrigation after the first water deficit cycle in the WS treatments did not allow soil moisture values to reach those of the WW treatments in any of the study plots.

3.2. *Crop temperature*

The crop temperatures determined from thermal imaging for all experimental plots at various flight altitudes and on six sampling dates during the irrigation season were averaged for each flight altitude to analyse the effect of height (from 5 to 40 m) on the estimated crop temperature. The mean crop temperatures of the four experimental plots averaged across the six flight dates were similar ($P > 0.05$) within the 5–40-m height range (Fig. 4).

The mean crop temperatures at 30 m were used to calculate the crop-air temperature differences (ΔT) and CWSI for each experimental plot throughout the study period (Fig. 5). A comparison of the ΔT dynamics derived for WW_{Clay} and WW_{Sand} showed that WW_{Sand} had lower ΔT values than WW_{Clay} at the beginning of the trial (DOY 85–115) and higher ΔT values from DOY 130 onwards (Fig. 5a). In the plots with irrigation deficits (WS), WS_{Sand} had lower ΔT values than those of WS_{Clay} at the beginning of the trial (DOY 85–115), but ΔT was consistently higher in WS_{Sand} than in WS_{Clay} from DOY 115 onwards (Fig. 5b). A comparison of the WW and WS plots for each soil type revealed that for the clay soil, ΔT was only slightly affected by the soil moisture differences (Fig. 3) caused by irrigation management. However, in the sandy soil, the ΔT of WS_{Sand} was substantially higher than that of WW_{Sand} from approximately DOY 115 (onset of the first water–stress cycle; Fig. 3). Similar seasonal trends to those described for ΔT were also observed for the CWSI (Fig. 5c and d). The CWSI values ranged from 0 to 1 across most of the experimental plots and sampling dates, but negative values observed in the sandy plots on one of the sampling days suggest that the NWSB from Idso (1982) may not be suitable for the prevailing environmental conditions of this study area.

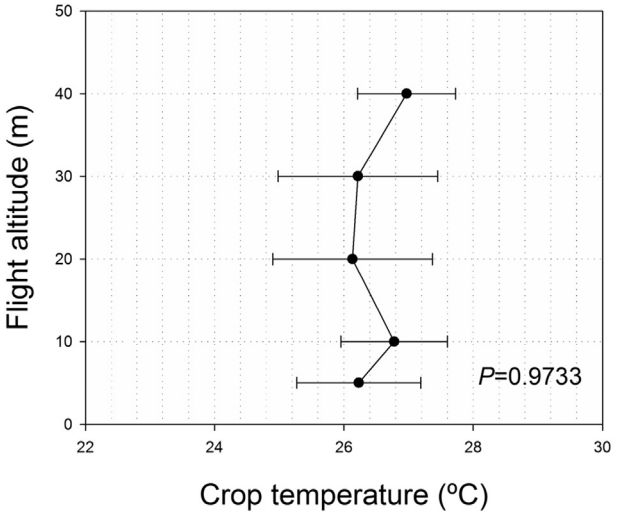

Fig. 4 – Crop temperatures determined at flight altitudes from 5 to 40 m. Each point represents the six-flight average of mean crop temperature determined for the four experimental plots. The error bars indicate the standard error of the mean.

Table 3 shows the sugar beet yield components determined at harvest for all experimental plots. Irrigation management had a significant effect on sugar beet yield in both soil types, although a more negative impact of water stress was observed in the sandy soil. In the clay soil, WS_{Clay} showed a significant decrease in fresh root mass compared to WW_{Clay}, but this reduction was not translated into a sugar content reduction since the sugar recovery rate of WS_{Clay} was significantly higher than that of WW_{Clay}. In the sandy soil, both the fresh root mass and sugar content were significantly lower in WS_{Sand} than in WW_{Sand}, while no differences in sugar recovery rate were observed in this soil type. The soil type had also a significant impact on sugar beet fresh root mass, as indicated by the lower values observed in both WW_{Clay} and WS_{Clay} than in the corresponding sandy plots. The soil type had no effect on the sugar content, as similar sugar contents were measured in WW_{Clay} and WW_{Sand} as well as in WS_{Clay} and WS_{Sand}.

In an attempt to integrate the cumulative water stress in the experimental plots during the measurement period, a WSI was calculated for all plots based on the ΔT measurements and an adaptation of the expression originally developed by Myers (1988) to quantify the cumulative integral of leaf water potential over any chosen period of time. The derived WSI was related to sugar beet yield (both fresh root mass and sugar content), as shown in Fig. 6. The fresh root mass and sugar content tended to decrease linearly with increasing WSI. However, while the relationship between the fresh root mass and WSI was poor ($R^2 = 0.28$), the WSI and sugar content were closely related, as shown by the high coefficient of determination of the linear regression ($R^2 = 0.94$).

4. Discussion

This study provides further evidence of the impact that soil variability may have on crop performance when it is not considered as an additional factor of the production system. A uniform water supply in a non-uniform sugar beet field with strong soil texture variability led to differences in the REW between the clayey and sandy zones that were irrigated to satisfy crop water requirements (WW_{Clay} and WW_{Sand}, respectively) (Fig. 3). The marked decrease in REW observed from DOY 80 to 125 in WW_{Clay} compared to that in WW_{Sand} (Fig. 3) indicates the importance of considering soil variability in irrigation supply decisions. Although clayey soils may retain more water than sandy soils, the soil moisture measured taken in the 0–1000-mm soil profile suggested that the plants grown in the WW_{Clay} plot extracted more soil water than those grown in the WW_{Sand} plot from DOY 80 to 125. Although crop growth measurements were not performed to support this hypothesis, the fraction of green vegetation or canopy cover (i.e., the fraction of ground covered by green

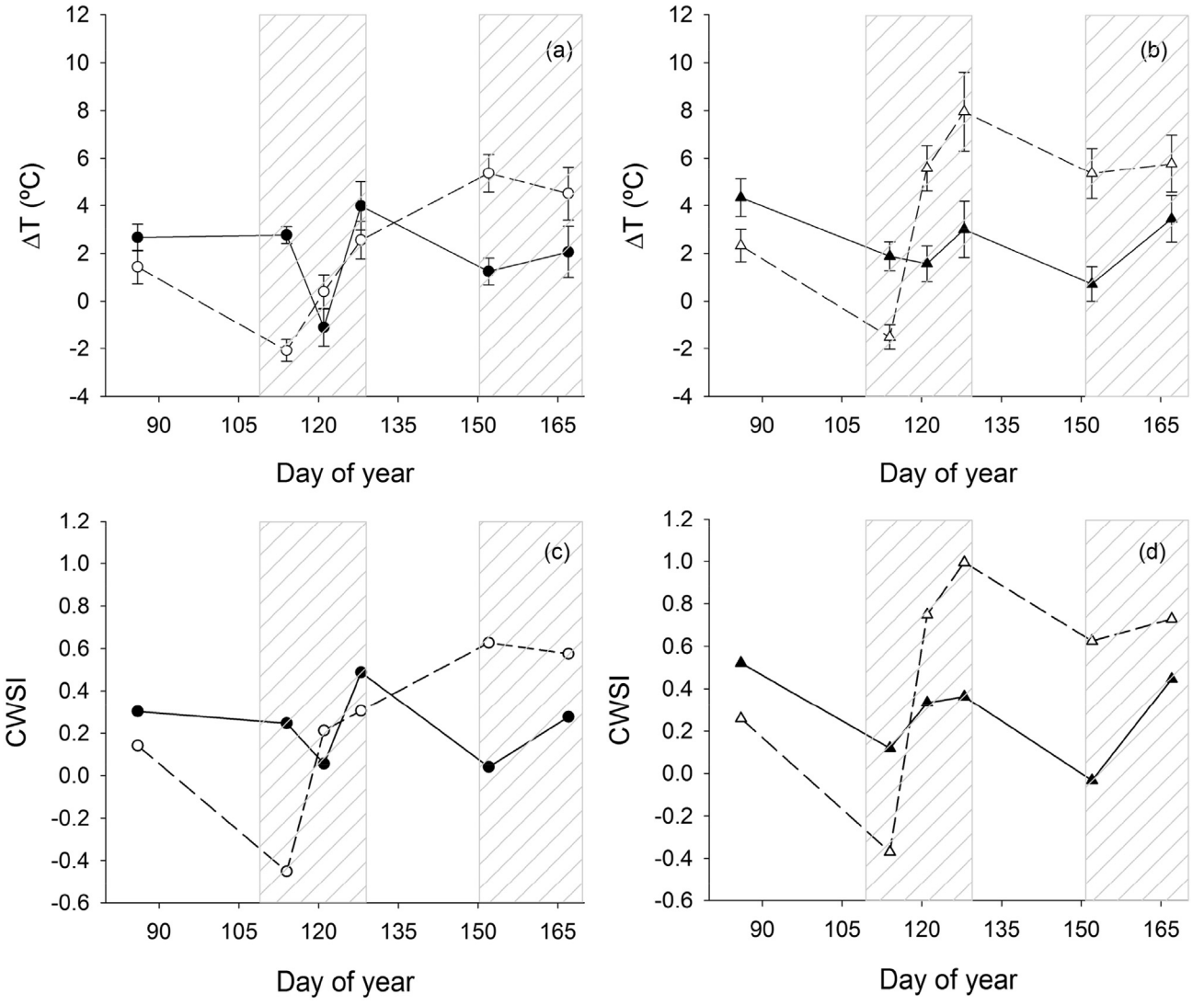

Fig. 5 – Evolution of the crop-air temperature difference (ΔT) and crop water stress index (CWSI) in WW_{Clay} and WW_{Sand} (a, c) and WS_{Clay} and WS_{Sand} (b, d) plots The crop temperature was measured at a flight altitude of 30 m. Error bars indicate the standard error of the mean. The hatched areas indicate the periods during which irrigation was withheld in the WS_{Clay} and WS_{Sand} sub-plots. Definition of symbols: filled triangles (WS_{Clay}), hollow triangles (WS_{Sand}), filled circles (WW_{Clay}), hollow circles (WW_{Sand}).

vegetation) estimated on DOY 86 for both WW plots from the thermal images captured using the micro-UAV (Fig. 7) revealed that the plants grown in the WW_{Clay} plot had 10% more canopy cover than the plants grown in the WW_{Sand} plot (see the caption of Fig. 7 for details on how plant cover was estimated). The faster canopy development observed in the WW_{Clay} plants can therefore explain the higher root water uptake observed in these plants compared with the WW_{Sand} plants.

Table 3 – Sugar beet yield components measured in the experimental plots.

Plot ID	Fresh root mass (t ha^{-1})	Sugar recovery (%)	Sugar content (t ha^{-1})
WW_{Clay}	104.0 ± 3.7b	14.8 ± 0.2b	15.4 ± 0.6a
WS_{Clay}	83.0 ± 1.5d	17.9 ± 0.3a	14.8 ± 0.3ab
WW_{Sand}	115.5 ± 4.3a	14.2 ± 0.1b	16.3 ± 0.6a
WS_{Sand}	93.2 ± 1.5c	14.6 ± 0.4b	13.6 ± 0.2b

Different letters within the same column denote significant differences based on Duncan's multiple range test.

Despite the valuable information provided by soil moisture sensors to support irrigation decisions, drawbacks of this technique in terms of acquiring accurate and representative soil moisture information have also been reported (Jones, 2004). The derivation of crop water stress indices from aerial thermal images represents a promising decision support tool to complement soil moisture information in irrigation programmes (Bellvert, Zarco-Tejada, Girona, & Fereres, 2014). The results obtained in this study suggest that during some periods of the sugar beet irrigation season, the soil moisture content determined from two probes per plot could not reproduce the dynamics of the derived thermal index, a

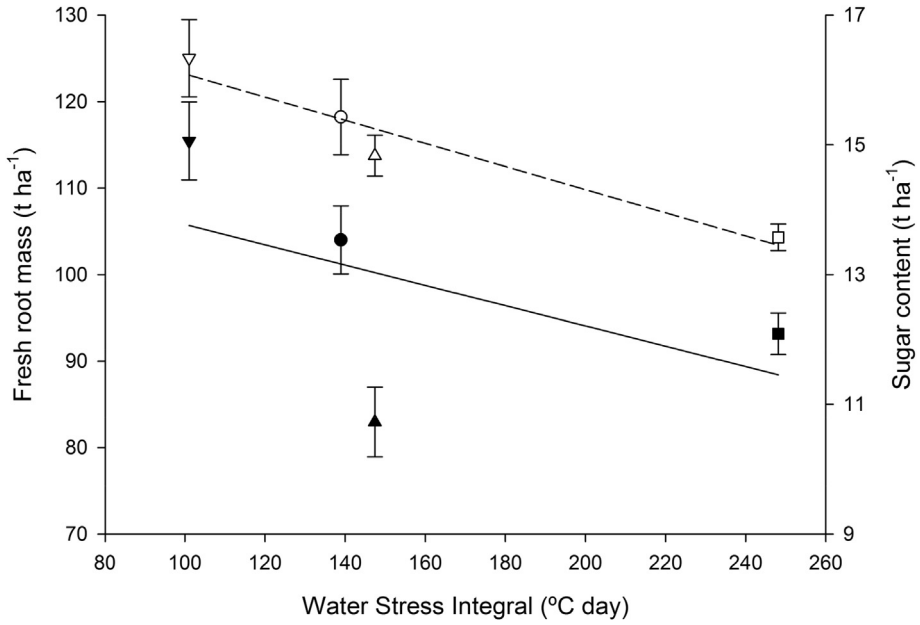

Fig. 6 – Relationships of the fresh root mass (filled symbols) and sugar content (hollow symbols) with the water stress integral (WSI) determined from the cumulative crop-air temperature difference. Dashed line: regression line between the sugar content and WSI ($y = 17.8–0.018x$, $R^2 = 0.94$). Continuous line: regression line between the fresh root mass and WSI ($y = 117.5–0.117x$, $R^2 = 0.28$). Definition of symbols: hollow symbols (sugar content), filled symbols (fresh root mass); triangles pointed upward (WS_{Clay}), inverted triangles (WW_{Sand}), circles (WW_{Clay}), squares (WS_{Sand}).

surrogate of crop transpiration. This was the case for the plants grown in the WS_{Sand} plots, which had higher REW values than the WS_{Clay} plants (Fig. 3). Moreover, the ΔT and CWSI values, which are used as proxies for the mean crop water stress (Maes & Steppe, 2012), were also higher in the WS_{Sand} than in the WS_{Clay} plots (Fig. 5) over the two cycles of imposed water stress. Furthermore, the WW_{Clay} and WW_{Sand} plots had similar REW values from DOY 150 onwards, while the corresponding mean ΔT and CWSI values were higher in the WW_{Sand} plants than in the WW_{Clay} plants. These findings highlight the differences in crop transpiration between the WW plots and suggest that soil moisture data measured in a small number of locations may not be reliable enough to represent the mean crop water status of zones with uniform soil properties. Poor relationships between canopy temperature-based indices and soil moisture deficits are frequently observed (DeJonge et al., 2015) and drive the search for remote sensing applications that use the crop as an

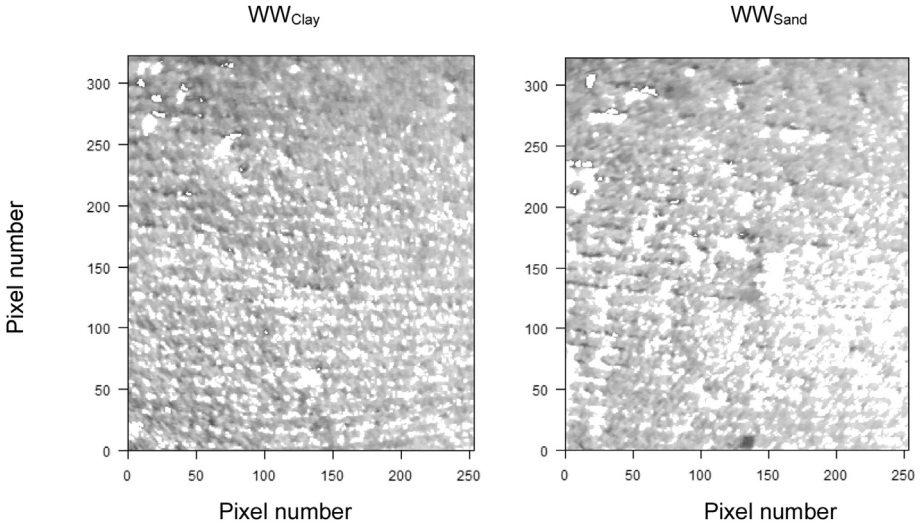

Fig. 7 – Thermal infrared images of the WW_{Clay} (left) and WW_{Sand} (right) plots with marked segments distinguishing between the background (soil) and regions of interest (vegetation). A segmentation algorithm based on the FWHM rule was applied. The IR thermal images were captured at a flight altitude of 20 m on day of year 86. Estimates of canopy cover were 90.77% and 80.96% in the WW_{Clay} and WW_{Sand} plots, respectively. WW indicates well-watered conditions.

intermediate sensor for quantifying soil water availability (Zhang, Clarke, Steven, & Jaggard, 2011).

Thermal indices derived from satellites and airborne observation platforms flying at high altitudes require complex post-processing to correct for parameters such as atmospheric transmissivity (Berni et al., 2009), which decreases with relative humidity, temperature and distance from the object (Sugiura, Noguchi, & Ishii, 2007). In arid and semi-arid regions, relatively stable atmospheric conditions prevail when thermal measurements are conducted at the same time of day under clear-sky conditions and during the months of high evaporative demand (irrigation season). This implies that thermal errors caused by variations in atmospheric transmissivity during low-altitude flights may be related to camera error. We assessed this possibility and found no significant differences in the mean crop temperature at flight altitudes of 0–40 m ($P = 0.9773$) (Fig. 4).

WSI values calculated from other non-thermal plant-based water stress indicators (e.g., predawn leaf water potential or stem water potential) and for different crop species showed great potential to predict yield losses due to water stress (Ginestar & Castel, 1996; Egea et al., 2013). The close relationship observed between sugar production and the temperature-based WSI (Fig. 6) indicates that T-based WSI was sensitive enough to capture the impacts of both soil heterogeneity and irrigation management on sugar production, thereby confirming the reliability of the method described in this work for monitoring the cumulative water stress in sugar beet fields.

From an irrigation scheduling perspective, use of CWSI as a crop water stress indicator for sugar beet requires further experimentation. Although this index is a sensitive indicator that is able to capture the differences between plants grown in sandy or clay soils and between well-watered plants and those subjected to intentional water shortages, aspects such as the derivation of a wet reference baseline adapted to Mediterranean conditions and local cultivars and the definition of threshold values for irrigation management based on relationships with other plant physiological variables (e.g., leaf gas exchange variables) need to be determined.

5. Conclusions

The results of this study yielded two clear conclusions. First, the canopy-air temperature differences and the CWSI values determined from thermal images captured using a micro-UAV were sensitive enough to identify variations in crop water use resulting from different irrigation management strategies or the natural variability of soil properties. Second, the dynamics of the soil moisture content determined from a limited number of sampling points (two probes per plot in this study) failed to adequately represent the variation in crop water use, as estimated from the thermal indices derived. This study presents a reliable method to monitor the spatio-temporal variations of crop water use in sugar beet fields, although further research is required to transform this information into optimal recommendations for sugar beet irrigation requirements. A temperature-based WSI was demonstrated to be a good predictor of the sugar content at harvest under both soil variability and irrigation management.

Acknowledgements

Financial support provided by the Spanish Ministry of Economy and Competitiveness (Research Project AGL2013-46343-R) and the Regional Government of Andalucía (Research Project P12-AGR-1227) is greatly appreciated.

REFERENCES

Allen, R. G., Pereira, L. S., Raes, D., & Smith, M. (1998). *Crop evapotranspiration—Guidelines for computing crop water requirements*. FAO Irrigation and drainage paper 56. Rome: Food and Agriculture Organization.

Beamish, D. (2011). Low induction number, ground conductivity metres: A correction procedure in the absence of magnetic effects. *Journal of Applied Geophysics, 75*(2), 244–253.

Bellvert, J., Zarco-Tejada, P. J., Girona, J., & Fereres, E. (2014). Mapping crop water stress index in a "Pinot-noir" vineyard: Comparing ground measurements with thermal remote sensing imagery from an unmanned aerial vehicle. *Precision Agriculture, 15*, 361–376.

Bellvert, J., Zarco-Tejada, P. J., Marsal, J., Girona, J., González-Dugo, V., & Fereres, E. (2016). Vineyard irrigation scheduling based on airborne thermal imagery and water potential thresholds. *Australian Journal of Grape and Wine Research, 22*, 307–315. http://dx.doi.org/10.1111/ajgw.12173.

Berni, J. A. J., Zarco-tejada, P. J., Suárez, L., & Fereres, E. (2009). Thermal and narrowband multispectral remote sensing for vegetation monitoring from an unmanned aerial vehicle. *IEEE Transactions on Geoscience and Remote Sensing, 47*, 722–738.

Blackmore, S., Godwin, R., & Fountas, S. (2003). The analysis of spatial and temporal trends in yield map data over six years. *Biosystems Engineering, 84*(4), 455–466.

Callegary, J. B., Ferre, T. P. A., & Groom, R. W. (2007). Vertical spatial sensitivity and exploration depth of low-induction-number electromagnetic-induction instruments. *Vadose Zone Journal, 6*(1), 158–167.

Cohen, Y., Alchanatis, V., Meron, M., Saranga, Y., & Tsipris, J. (2005). Estimation of leaf water potential by thermal imagery and spatial analysis. *Journal of Experimental Botany, 56*, 1843–1852.

Corwin, D. L., & Lesch, S. M. (2005). Characterizing soil spatial variability with apparent soil electrical conductivity: I. Survey protocols. *Computers and Electronics in Agriculture, 46*, 103–133.

Cox, P. G. (1996). Some issues in the design of agricultural decision support system. *Agricultural Systems, 52*(2–3), 355–381.

DeJonge, K. C., Taghvaeian, S., Trout, T. J., & Comas, L. H. (2015). Comparison of canopy temperature-based water stress indices for maize. *Agricultural Water Management, 156*, 51–62.

Delefortrie, S., Saey, T., Van De Vijver, E., De Smedt, P., Missiaen, T., Demerre, I., et al. (2014). Frequency domain electromagnetic induction survey in the intertidal zone: Limitations of low-induction-number and depth of exploration. *Journal of Applied Geophysics, 100*, 14–22.

Egea, G., Nortes, P. A., Domingo, R., Baille, A., Pérez Pastor, A., & González-Real, M. M. (2013). Almond agronomic response to long-term deficit irrigation applied since orchard establishment. *Irrigation Science, 31*, 445–454.

Fabeiro, C., Martin de Santa Olalla, C., Lopez, R., & Dominguez, A. (2003). Production and quality of the sugar beet (*Beta vulgaris* L.) cultivated under controlled deficit irrigation conditions in a semi-arid climate. *Agricultural Water Management, 62*, 215–227.

Ginestar, C., & Castel, J. R. (1996). Responses of young clementine citrus trees to water stress during different phonological periods. *Journal of Horticultural Science, 71*, 551–559.

Gonzalez-Dugo, M. P., Moran, M. S., Mateos, L., & Bryant, R. (2006). Canopy temperature variability as an indicator of crop water stress severity. *Irrigation Science, 24*, 233–240.

Goovaerts, P. (1997). Geostatistics for natural resources evaluation. In *Applied geostatistics series*. New York: Oxford University Press.

Idso, S. B. (1982). Non-water stressed baselines: A key to measuring and interpreting plant water stress. *Agriculture Meteorology, 27*, 59–70.

Idso, S. B., Jackson, R. D., Pinter, P. J., Reginato, R. J., & Hatfield, J. L. (1981). Normalizing the stress-degree-day parameter for environmental variability. *Agriculture Meteorology, 24*, 45–55.

Jackson, R. D., Idso, S. B., Reginato, R. J., & Pinter, P. J. (1981). Canopy temperature as a crop water-stress indicator. *Water Resources Research, 17*, 1133–1138.

Jones, H. G. (1992). *Plants and microclimate* (2nd ed.). Cambridge: Cambridge University Press.

Jones, H. G. (2004). Irrigation scheduling: advantages and pitfalls of plant-based methods. *Journal of Experimental Botany, 55*, 2427–2436.

Käthner, J., Ben-Gal, A., Gebbers, R., Peeters, A., Herppich, W. B., & Zude-Sasse, M. (2017). Evaluating spatially resolved influence of soil and tree water status on quality of European plum grown in semi-humid climate. *Frontiers in Plant Science, 8*, 1053. http://dx.doi.org/10.3389/fpls.2017.01053.

Krishna, K. R. (2016). *Push button agriculture: Robotics, drones, satellites-guided soil and crop management*. Oakville (Canada): Apple Academic Press, Inc.

Lopéz-Moreno, J. I., Vicente-Serrano, S. M., Beguería, S., García-Ruiz, J. M., Portela, M. M., & Almeida, A. B. (2009). Dam effects on droughts magnitude and duration in a transboundary basin: The lower River Tagus, Spain and Portugal. *Water Resources Research*, 45, W02405. http://dx.doi.org/10.1029/2008WR007198.

Maes, W. H., & Steppe, K. (2012). Estimating evapotranspiration and drought stress with ground-based thermal remote sensing in agriculture: A review. *Journal of Experimental Botany, 63*, 4671–4712.

McNeill, J. D. (1980). *Electromagnetic terrain conductivity measurement at low induction numbers*. Technical Note TN-6. Mississauga, ON, Canada: Geonics Ltd..

Möller, M., Alchanatis, V., Cohen, Y., Meron, M., Tsipris, J., Naor, A., et al. (2007). Use of thermal and visible imagery for estimating crop water status of irrigated grapevine. *Journal of Experimental Botany, 58*, 827–838.

Myers, B. J. (1988). Water stress integral-a link between short-term stress and long-term growth. *Tree Physiology, 4*, 315–323.

Payero, J. O., Tarkalson, D., & Irmak, S. (2006). *Corn yield response to different irrigation depths with subsurface drip irrigation*. Omaha, Nebraska: World Environmental and Water Resources Congress 2006.

Qi, Z., & Helmers, M. J. (2010). The conversion of permittivity as measured by a PR2 capacitance probe into soil moisture values for Des Moines lobe soils in Iowa. *Soil Use and Management, 26*, 82–92.

Rud, R., Cohen, Y., Alchanatis, V., Beiersdorf, I., Klose, R., Presnov, E., et al. (2015). Characterization of salinity-induced effects in olive trees based on thermal imagery. In *Precision agriculture 2015 - Pap. Present. 10th Eur. Conf. Precis. Agric. ECPA 2015* (pp. 511–517).

Rud, R., Cohen, Y., Alchanatis, V., Levi, A., Brikman, R., Shenderey, C., et al. (2014). Crop Water Stress Index derived from multi-year ground and aerial thermal images as an indicator of potato water status. *Precision Agriculture, 15*, 273–289.

Scholander, P. F., Hammel, H. T., Bradstreet, E. D., & Hemmingsen, E. A. (1965). Sap pressure in vascular plants. *Science, 148*, 339–346.

Snyder, W., & Wan, Z. (1998). BRDF models to predict spectral reflectance and emissivity in the thermal infrared. *IEEE Transactions on Geoscience and Remote Sensing, 36*(1), 214–225.

Sugiura, R., Noguchi, N., & Ishii, K. (2007). Correction of low-altitude thermal images applied to estimating soil water status. *Biosystems Engineering, 96*, 301–313.

Taghvaeian, S., Comas, L., DeJonge, K. C., & Trout, T. J. (2014). Conventional and simplified canopy temperature indices predict water stress in sunflower. *Agriculture Water Management, 144*, 69–80.

Testi, L., Goldhamer, D. A., Iniesta, F., & Salinas, M. (2008). Crop water stress index is a sensitive water stress indicator in pistachio trees. *Irrigation Science, 26*, 395–405.

Van Genuchten, M. T. (1980). A closed-form equation for predicting the hydraulic conductivity of unsaturated soils. *Soil Science Society of America Journal, 44*, 892–898.

Zhang, L., Clarke, M. L., Steven, M. D., & Jaggard, K. W. (2011). Spatial patterns of wilting in sugar beet as an indicator for precision irrigation. *Precision Agriculture, 12*, 296–316.

Zude-Sasse, M., Fountas, S., Gemtos, T. A., & Abu-Khalaf, N. (2016). Applications of precision agriculture in horticultural crops. *European Journal of Horticultural Science., 81*(2), 78–90.